DOI: 10.1002/chem.201002228

Oriented Free-Standing Ammonium Vanadium Oxide Nanobelt Membranes: Highly Selective Absorbent Materials

Rujia Zou, Zhenyu Zhang, Li Yu, Qiwei Tian, Jianghong Wu, Yangang Sun, Zhigang Chen, and Junqing Hu*[a]

Abstract: Highly selective, absorbent, free-standing, paper-like membranes made of ammonium vanadium oxide ($NH_4V_4O_{14}$) nanobelts have been engineered by taking advantage of the nanoscaled self-assembly of architectures that display a mesh structure with an average periodic pore size of about 5 to 10 nm. The $NH_4V_4O_{14}$ nanobelts are synthesized by using a simple hydrothermal process, and exhibit the same orientation and assemble into bundles, each about 40 to 80 nm in width, 3 to 5 nm in thickness, and up to several millimeters in length. Importantly, the as-obtained $NH_4V_4O_{14}$ nanobelt membranes can highly selectively absorb a variety of organic solvents, covering both polar and non-polar solvents, for example, the absorbent capacity of glycol is 28 times as high as the initial weight of the membrane, and it can even separate organic solvents with similar polarities and absorb solid contaminants in organic solvents. These highly selective, absorbent membrane materials can be an ideal candidate for the separation and removal of pollution in industrial and environmental applications.

Keywords: absorption · hydrophobic effect · membranes · nanostructures · vanadium

Introduction

The lotus leaf effect, that is, superhydrophobicity, is a surface phenomenom that demonstrates self-cleaning and can condense water from dry environments. Inspired by this enlightening natural phenomenon in nanotechnology, scientists have developed a variety of synthetic materials that show superwetting behavior for potential applications in many fields.[1–9] An extraordinary array of approaches, including the topological construction of micro- and nanostructures,[10–13] surface modification with low-surface-energy molecules,[14] and utilization of stimuli-responsive materials,[15–17] have been developed to alter the wettability of a material.[18–21] The wettability of the materials in the majority of these approaches, however, is firmly linked to the supporting substrate and thus a structure consisting of a wetting material and substrate is regarded as an integrated system. In contrast, a strategy that leads to an easily scalable procedure to create a large-scale free-standing structure for practical applications is a substantial challenge because assembly methods that simultaneously control the wetting properties and structure at the macroscale dimensions remain elusive.[22,23] So far, free-standing structures, such as layer-by-layer assembled polymer films,[19] carbon nanotube membranes,[25,26] metallic nanoparticle monolayers[27] and other inorganic materials sheets,[28–31] and protein-based membranes,[32] have been reported. However, they have limitations for practical applications that require low-cost and large-scale fabrication, high thermal stability, and a wide range of wetting behavior for both polar and non-polar solvents. In our previous study, we created free-standing superhydrophobic membranes from potassium manganese oxide nanowires with good selectivity and the capacity to separate oil from water.[33]

Herein, by taking advantage of the high internal surface area and the nanoscaled self-assembly of architectures, we have engineered new highly selective, absorbent free-standing, paper-like membrane materials composed of ammonium vanadium oxide ($NH_4V_4O_{14}$) nanobelts. The as-obtained $NH_4V_4O_{14}$ nanobelt membranes can selectively absorb a variety of both polar and non-polar organic solvents, for exam-

[a] R. Zou,[+] Z. Zhang,[+] L. Yu, Q. Tian, J. Wu, Dr. Y. Sun, Dr. Z. Chen, Prof. Dr. J. Hu
State Key Laboratory for Modification of Chemical Fibers and Polymer Materials
College of Materials Science and Engineering
Donghua University, Shanghai 201620 (China)
Fax: (+86) 21-67792855
E-mail: hu.junqing@dhu.edu.cn

[+] These authors contributed equally to this work.

Supporting information for this article is available on the WWW under http://dx.doi.org/10.1002/chem201002228.

ple, the absorbent capacities of glycol can be up to 28 times as high as the initial weight of the nanobelts. Moreover, these selectively absorbent membranes can even separate two mixed solvents with very similar polarities and absorb solid contaminants in organic solvents. Therefore, these highly selective, absorbent materials may provide a blueprint that can guide the design of future nanomaterials for environmental applications.

Results and Discussion

The inset of Figure 1a shows the large amount of dark-green floccules that were obtained during the synthesis of the nanobelts. Interestingly, the as-obtained product naturally

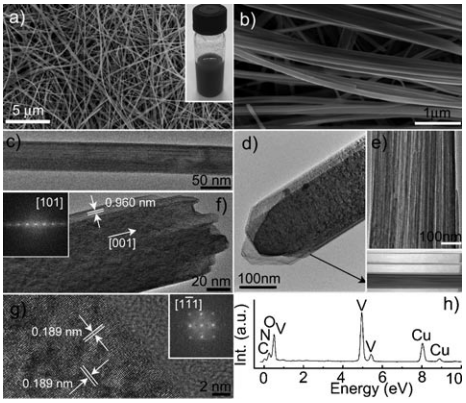

Figure 1. Characterization of $NH_4V_4O_{14}$ nanobelts. a) SEM image of the $NH_4V_4O_{14}$ nanobelts; inset: the dark-green floccules. b) High-magnification SEM image of a nanobelts bundle. c) TEM image of a single nanobelt. d) TEM image of the nanobelt bundle from the top. e) TEM image of the nanobelts bundle from the side; inset: the layered appearance of the nanobelts. f) HRTEM image of the nanobelt showing the [001] growth direction; inset: the FFT pattern along the [101] axis. g) HRTEM image of the nanobelt; inset: the FFT pattern along the [1$\bar{1}$1] axis. h) Typical EDS spectrum taken from a selected area in c).

existed in the form of a membrane in the autoclave (see Figure S1, Supporting Information). A low-magnification SEM image (Figure 1a) shows that the product consists of a large quantity of straight and twisted nanobelts, with lengths of up to several hundreds of micrometers and even up to the millimeter scale. A highly magnified SEM image (Figure 1b) indicates that these belts are assembled into a large number of bundles; assembled bundles can have lengths of several millimeters or greater. The TEM image in Figure 1c reveals that each belt has a uniform width and thickness along its entire length, and the typical width and thickness of the belts are in the range of 40 to 80 nm and 3 to 5 nm, respectively. In fact, each bundle is composed of dozens of nanobelts, as shown by TEM images from the top (Figure 1d) and side (Figure 1e). Within a bundle, the constituent belts overlap or arrange side by side (see Figure S2, Supporting Information) and have uniform width and orientation throughout the whole length, appearing in a layered arrangement with an average periodic pore size of about 5 to 10 nm, as shown in Figure 1e, inset. As seen from a high-resolution TEM (HRTEM) image of the belt (Figure 1f), the belts are composed of regularly ordered molecular layers; the edge of the ribbon is clean and very abrupt on the atomic scale and there are no amorphous layers covering the surface. The lattice fringes of the (001) planes with a *d* spacing of 0.931 nm can be clearly seen, and growth is in the [001] direction, that is, along the *c* direction of the belt (indicated by an arrow). The fast Fourier transform (FFT) image (Figure 1f, inset) shows a typical pattern along the [101] axis of the belt. This indicates that the nanobelt grew along the [001] direction. Diffraction patterns taken from different parts of the nanobelt show exactly the same pattern without further tilting of the nanobelt, which indicates the single-crystal nature of the whole nanobelt. Examination of several tens of individual nanobelts suggest that all of them grew along the [001] direction. Figure 1g shows another HRTEM image of the belt, in which the belt is structurally uniform and no dislocations or other planar defects were observed in all areas examined, and the measured *d* spacings of 0.189 nm correspond to the (−314) lattice fringes of the ammonium vanadium oxide ($NH_4V_4O_{14}$) crystal, respectively. The FFT pattern (Figure 1f, inset) is coincident with the [1$\bar{1}$1] axis pattern of the crystal. Extensive HRTEM and FFT examinations indicate that the structural uniformity of the single-crystal nanobelt is maintained along the entire length. A typical X-ray energy dispersive spectrum (EDS; Figure 1h) confirms that the nanobelts have a chemical composition of O, N, and V (C and Cu signals originate from the TEM grid).

Figure 2a and b show comparative X-ray diffraction (XRD) patterns of the as-synthesized $NH_4V_4O_{14}$ nanobelts and the $NH_4V_4O_{14}$ powders from the Joint Committee on Powder Diffraction Standards (JCPDS) card (31-0075), respectively. Interestingly, the XRD patterns of the $NH_4V_4O_{14}$ nanobelts only display a series of 00*l* diffraction peaks, whereas other characteristic peaks are absent. The four peaks can be assigned to be the first, second, third, and

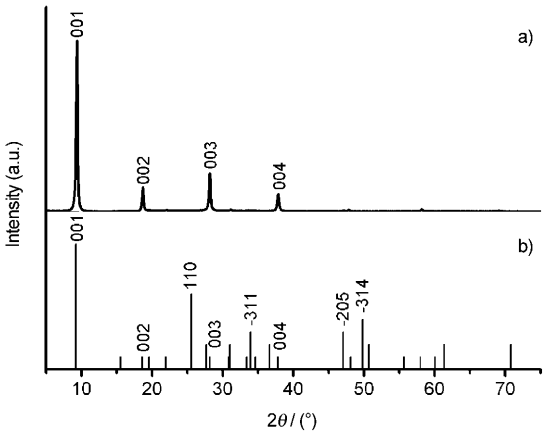

Figure 2. XRD patterns of a) the as-synthesized $NH_4V_4O_{14}$ nanobelts. b) $NH_4V_4O_{14}$ powders from the JCPDS card (31-0075).

fourth-order peaks of the (001) crystal plane, respectively, which indicates a preferential orientation in the *c* direction. The interlayer *d* spacings of the $NH_4V_4O_{14}$ structure were calculated to be 0.938, 0.472, 0.316, and 0.237 nm for (001) ($2\theta = 9.36°$), (002) ($2\theta = 18.7°$), (003) ($2\theta = 28.16°$), and (004) ($2\theta = 37.84°$), respectively. These diffraction peaks were indexed as the $NH_4V_4O_{14}$ monoclinic phase within the experimental error (JCPDS card 31-0075: $a = 52.665$, $c = 54.947$ Å). No characteristic peaks peculiar to the starting materials or other impurities were observed. Thus, it is concluded that the as-synthesized $NH_4V_4O_{14}$ nanobelts exhibit a well-defined (00l) crystal plane orientation. These XRD results agree well with the HRTEM imaging and FFT patterns shown in Figure 1d and e. This novel orientation is attributed to the self-assembly of the $NH_4V_4O_{14}$ nanobelts into a membrane.

A suspension of as-synthesized $NH_4V_4O_{14}$ nanobelts and alcohol was formed by ultrasonic dispersion, and the alcohol was subsequently removed by casting the suspension on a glass substrate placed in an oven at 60 °C to give a self-assembled free-standing, paper-like nanobelt membrane (see Figure S3, Supporting Information). The nanobelt membranes have uniform surface morphology and homogenous thickness and, importantly, can be formed with an arbitrary area size; a sample of the $NH_4V_4O_{14}$ nanobelt membrane with a diameter of 12 cm is shown in Figure 3a. The mechanical flexibility of individual $NH_4V_4O_{14}$ nanobelts and the strong binding between these nanobelts account for the strong adhesion of the nanobelt paper (Figure 3a, inset). Within the membrane, the $NH_4V_4O_{14}$ nanobelts arrange in a crisscrossed manner to form a network or a mesh structure with an average periodic rectangular pore size of about 5 to 10 nm (see Figure 1d and e and Figure S4, Supporting Information). The network or mesh structure is maintained across the whole membrane, as shown in Figure 3b. A typical cross-sectional SEM image (Figure 3c) shows a layered membrane (≈ 80 μm thick), in which the number of layers corresponds to the number of castings.

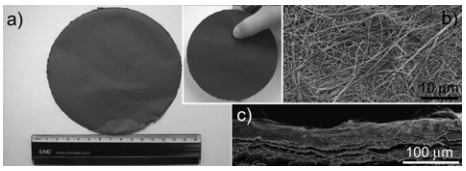

Figure 3. Characterization of the as-synthesized nanobelt membranes. a) Photograph of the paper-like $NH_4V_4O_{14}$ membrane; inset: the vertical free-standing, paper-like membrane. b) SEM image showing the surface morphology of the membrane. c) Cross-sectional SEM image of the membrane.

A contact angle (CA) was measured to examine the wettability of the $NH_4V_4O_{14}$ nanobelt membranes. The wetting time was as short as 0.07 s for a droplet (2 μL) of water added to the membrane surface. This phenomenon indicates that the nanobelt membrane is superhydrophilic in the bulk of this material. To obtain superhydrophobic surfaces, we created homogenous coatings on the entire surfaces of the $NH_4V_4O_{14}$ nanobelt membrane by using a vapor-deposition technique.[34] Typically, the nanobelt membrane was placed in a container with silicone oil DC-200 and heated at 240 °C for 20 min. After this heat treatment, individual $NH_4V_4O_{14}$ nanobelts in the membrane were coated with silicone molecules. The SEM image (Figure 4a) reveals that the

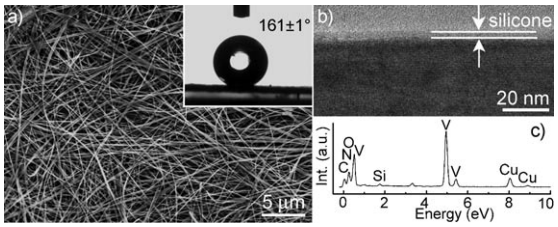

Figure 4. Characterization of the silicone-coated $NH_4V_4O_{14}$ nanobelt membrane. a) SEM image of the silicone-coated nanobelts; inset: the water CA measurement of the silicone-coated membrane. b) TEM image of the silicone coating on a nanobelt. c) EDS spectrum taken from a selected area in b).

$NH_4V_4O_{14}$ nanobelts coated with silicone molecules were still as uniform as nanobelts without silicone molecule coatings. The wetting behavior of the silicone-coated nanobelt membrane was evaluated by water CA measurements. The CA of water on the membrane was measured to be $160 \pm 1°$ (Figure 4a, inset), which indicates that the membrane surface is superhydrophobic.[35–37] Importantly, the silicone-coated $NH_4V_4O_{14}$ nanobelt membrane maintains its superhydrophobicity even after being immersed in water at room temperature for a long time (several months). Comparative experiments on other materials, such as Si wafers and SnO_2 nanobelt films exposed to the same silicone-coating treatment, produced surfaces with a CA of less than 125°, which confirms that the silicone coating itself is not the sole cause of the high CA of the $NH_4V_4O_{14}$ membrane (see Figure S5, Supporting Information). It is known that the unusual wetting characteristics of hydrophobic surfaces are mainly governed by their surface free energy and surface structure.[34–36] These results indicate that the $NH_4V_4O_{14}$ nanobelt structures strongly enhanced the hydrophobicity. The $NH_4V_4O_{14}$ nanobelt structures dramatically increase the surface roughness of the films, which means that air can be trapped in the gaps of these highly oriented nanostructured surfaces. Thus, it is reasonable that clean, self-assembled, and free-standing architectures are result of high CA. As seen in Figure 4b, the silicone coating on the nanobelt is about 2 to 3 nm thick and homogenous throughout the whole belt. Composition analysis of the nanobelt by using EDS (Figure 4c) reveals the presence of silicon as well as O, N, and V from the original nanobelt.

The silicone-coated $NH_4V_4O_{14}$ nanobelts membrane shows highly selective absorption of a variety of organic solvents. When the $NH_4V_4O_{14}$ nanobelt membrane comes into contact with a layer of toluene on water, it quickly absorbs toluene but repels the water (see the Supporting Informa-

tion movie). It is known that polypropylene and glass fabric membranes both exhibit absorbence toward both water and toluene, whereas the superhydrophobic membrane only absorbs toluene. Alternatively, it is the unique superwetting surface that makes the membrane a selective absorption material. Most importantly, the $NH_4V_4O_{14}$ nanobelt membrane possesses high absorption capacity. For example, the membrane (2×2 cm) shows an uptake capacity of up to 24 times its weight for toluene on water in a very short absorption time (<10 s; Figure 5a and b). A combination of wettability

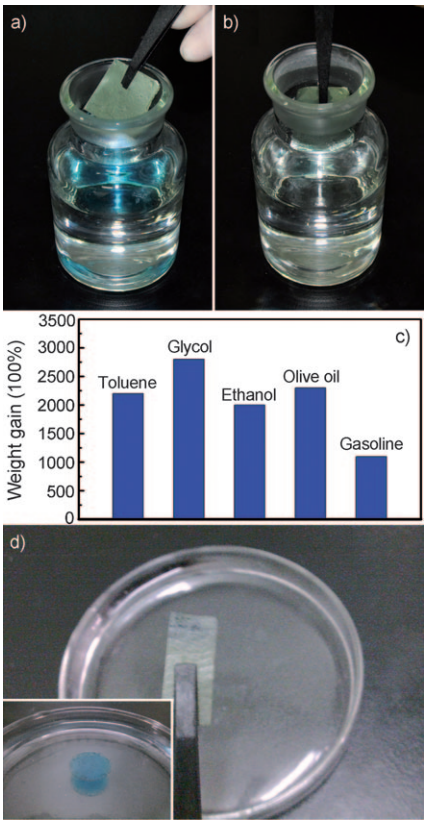

Figure 5. Absorption studies of the silicone-coated nanobelt membranes. a, b) A layer of benzene can be removed from the water surface by immersing the membrane. The toluene was labeled with Oil Blue 35 dye for clarity. c) Absorption capacities of the membrane toward organic solvents and oils expressed in terms of the weight gain. d) Toluene and solid contaminations can be removed instantaneously by the membrane; inset: droplets of toluene and solid contaminants on water.

properties with strong capillary effect due to the highly periodic rectangular porous architecture inside the $NH_4V_4O_{14}$ nanobelts and the high internal interspace of the membrane results in extraordinary selectivity and capacity for the separation of toluene from water. It is known that the absorbency of a membrane depends on good capillary action. Normally, a microstructure with a smaller barrier shows better capillary action than that with an arbitrary microstructure. The capillary action (H_0) of the rectangular pores can be represented by Equation (1):[38–40]

$$H_0 = \frac{(\sigma_{13} - \sigma_{23})l}{\rho g S} = \frac{\sigma_{12} l \cos\theta}{\rho g S} \quad (1)$$

in which σ_{12} is the local tension coefficient of the gas and liquid surface, θ is the angle of the rectangular pores and the liquid surface, l is the perimeter of a rectangular pore and S is the area of a rectangular pore [Eq. (2)], and ρ and g are constants.

$$\begin{aligned} l &= 2(a+b) \\ S &= ab \end{aligned} \quad (2)$$

a and b are the length and width, respectively, of a rectangular pore. Combining Equations (1) and (2) gives Equation (3):

$$H_0 = \frac{\sigma_{12}}{\rho g}\left[\frac{1}{a/(2\cos\theta)} + \frac{1}{b/(2\cos\theta)}\right] \quad (3)$$

In the present case, as suggested by TEM images and FFT patterns, the $NH_4V_4O_{14}$ nanobelts are structurally uniform single crystals with no dislocations or other planar defects; the surfaces of the $NH_4V_4O_{14}$ nanobelts are very clean. As a result, for a given material with highly periodic rectangular porous microstructures, the width (b) is a very small and contributes significantly to the capillary action. This is the reason that the membranes have outstanding absorbency and a short absorption time. Additionally, as shown in Figure 5c, the membrane also has a very strong capacity for absorbing various organic solvents or oil from water, even from surfactant-stabilized emulsions. In another example, the capacity of the membranes to absorb glycol is 28 times as high as the initial weight of the membranes. Most interestingly, the $NH_4V_4O_{14}$ superwetting membrane has the capacity to instantaneously absorb solid contaminants in organic solvent, as shown in Figure 5d. Another major advantage of the $NH_4V_4O_{14}$ nanobelts membrane is its thermal stability; it is stable at temperatures up to 280 °C (see Figure S6, Supporting Information). The absorbed organic solvent in the membrane can be removed by autoclaving, which means that recycling of the absorbed membrane is possible. These highly selective, absorbent properties make this $NH_4V_4O_{14}$ membrane an ideal candidate for the separation and removal of pollution in industrial and environmental applications.

Interestingly, not only can the $NH_4V_4O_{14}$ nanobelt membrane selectively collect oil and not water, it can even separate organic solvents with similar polarity, such as highly toxic benzene and its less-toxic close relative, toluene. A typical procedure for solvent separation is as follows: A superhydrophobic nanobelt membrane was dipped into a 1:1 (v/v) mixture of toluene and benzene. The tip of a large piece of nanobelt membrane (Figure 6, inset, a) was immersed into a mixture of toluene and benzene for 2 min, then the membrane was removed from the solvent and cut into five small pieces of equal length (4×5 mm; Figure 6, inset), and subsequently placed in separate vials that con-

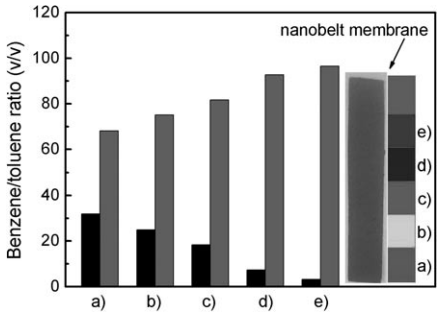

Figure 6. A typical procedure showing the separation of a mixture of toluene (gray bars) and benzene (black bars), which have very similar polarities. The molar ratios of the solvents absorbed on five pieces a)–e) cut from the nanobelt membrane were calculated by using gas chromatography. Inset: The five equally sized pieces a)–e).

tained acetone (2 mL) for gas chromatography. As shown in Figure 6, the calculated molar ratios of toluene and benzene from the solvents absorbed on the five pieces of membrane were 68:32, 75:25, 82:18, 93:7, and 97:3. Despite the very similar polarity of toluene and benzene, we were able to obtain a solvent ratio of at least 95:5 (v/v; toluene/benzene) after 2 min absorption of the mixed solvents. Due to the nanoscopic and highly periodic porous architecture inside the $NH_4V_4O_{14}$ nanobelts and the high internal interspace of the membrane, subtle adhesion difference between the solvent systems and capillary force in the membrane can be amplified in a mixture of two solvents. As a result, a tremendous variation in the ratio of the solvents absorbed occurred as the solvent mixture rose from the bottom to the top of the nanobelt membrane. Thus, the membranes have the possibility of separating one solvent from a mixture of two solvents with very similar polarities. A more immediate application for these $NH_4V_4O_{14}$ membrane materials will be the removal of hydrophobic contaminants with very similar polarities. This study may prove particularly useful in the design of recyclable separations with significant environmental applications.

Conclusion

Highly selective, absorbent, free-standing, paper-like, highly oriented membranes composed of ammonium vanadium oxide ($NH_4V_4O_{14}$) nanobelts have been created by taking advantage of the nanoscaled self-assembly of the architecture, and exhibit controllable wetting behavior ranging from superhydrophilic to superhydrophobic (when coated with silicone molecules). The as-obtained $NH_4V_4O_{14}$ nanobelt membranes can selectively absorb a variety of both polar and non-polar organic solvents; moreover, they can even separate two mixed solvents with very similar polarities and absorb solid contaminants in organic solvents. This extraordinary selectivity and strong absorbance capacity are due to the high internal interspaces and highly periodic rectangular porous architecture of the $NH_4V_4O_{14}$ nanobelts. Additionally, the membranes show high thermal stability and good recyclability. Our results suggest that this $NH_4V_4O_{14}$ nanobelt membrane material should find practical applications in industrial and environmental applications, such as in the field of oil spill cleanup.

Experimental Section

Ammonium vanadium oxide ($NH_4V_4O_{14}$) nanobelts were synthesized under hydrothermal conditions. All chemicals were purchased from Sinopharm Chemical Reagent Co. (Shanghai, China) and were used without further purification. In a typical synthesis, ammonium metavanadate (0.351 g) was dissolved in deionized water to form an ivory-white clear solution. Acetic acid was added dropwise with stirring to the ammonium metavanadate solution (45 mL) until the final pH of the solution was about 4.5 and a clear orange solution was formed. This solution was transferred into a Teflon-lined autoclave (50 mL) with a stainless-steel shell, which was kept at 190 °C for 36 h and then allowed to cool to RT. Interestingly, the final product naturally formed as a membrane in the Teflon-lined autoclave. This membrane was washed with deionized water and pure alcohol several times to remove any possible residues. Finally, a suspension of as-obtained $NH_4V_4O_{14}$ nanobelts and pure alcohol was formed by ultrasonic dispersion, and the alcohol was subsequently removed by casting the suspension on a glass substrate placed in an oven at 60 °C to give self-assembled free-standing paper-like nanobelt membranes.

Powder X-ray diffraction (XRD) experiments were conducted by using a D/max-2550 PC X-ray diffractometer (Rigaku, Japan). The morphologies and structures of the $NH_4V_4O_{14}$ nanobelts were characterized by using a field-emission scanning electron microscope (S-4800), and a transmission electron microscope (JEM-2010F). Contact angles were measured by using an OCA40 Micro contact-angle system (Dataphysics, Germany) at ambient temperature. Organic compositions were analyzed by using a QP-2010 gas chromatography system (Shimadzu, Japan).

Acknowledgements

This work was supported from the National Natural Science Foundation of China (Grant No. 50872020 and 50902021), the Program for New Century Excellent Talents of the University in China, the "Pujiang" Program of Shanghai Education Commission (Grant No. 09P51400500), the Science and Technology Commission of Shanghai-based "Innovation Action Plan" Project (Grant No. 10JC1400100), the "Dawn" Program of the Shanghai Education Commission (Grant No. 08SG32), the "Chen Guang" project (Grant No. 09CG27) supported by the Shanghai Municipal Education Commission and Shanghai Education Development Foundation, the Shanghai Leading Academic Discipline Project (Grant No. B603), and the Program of Introducing Talents of Discipline to Universities (No. 111-2-04).

[1] A. Nakajima, K. Hashimoto, T. Watanabe, K. Takai, G. Yamauchi, A. Fujishima, *Langmuir* **2000**, *16*, 7044–7047.
[2] R. Blossey, *Nat. Mater.* **2003**, *2*, 301–306.
[3] H. Y. Erbil, A. L. Demirel, Y. Avci, O. Mert, *Science* **2003**, *299*, 1377–1380.
[4] L. Zhai, F. C. Cebeci, R. E. Cohen, M. F. Rubner, *Nano Lett.* **2004**, *4*, 1349–1353.
[5] K. Acatay, E. Simsek, C. Ow-Yang, Y. Z. Menceloglu, *Angew. Chem.* **2004**, *116*, 5322–5325; *Angew. Chem. Int. Ed.* **2004**, *43*, 5210–5213.
[6] D. L. Tian, Q. W. Chen, F. Q. Nie, J. J. Xu, Y. L. Song, L. Jiang, *Adv. Mater.* **2009**, *21*, 3744–3749.

[7] L. Jiang, Y. Zhao, J. Zhai, *Angew. Chem.* **2004**, *116*, 4438–4441; *Angew. Chem. Int. Ed.* **2004**, *43*, 4338–4341.
[8] T. L. Sun, G. J. Wang, L. Feng, B. Q. Liu, Y. M. Ma, L. Jiang, D. B. Zhu, *Angew. Chem.* **2004**, *116*, 361–364; *Angew. Chem. Int. Ed.* **2004**, *43*, 357–360.
[9] T. C. Merkel, B. D. Freeman, R. J. Spontak, Z. He, I. Pinnau, P. Meakin, A. J. Hill, *Science* **2002**, *296*, 519–522.
[10] D. Y. Ryu, K. Shin, E. Drockenmuller, C. J. Hawker, T. P. Russell, *Science* **2005**, *308*, 236–239.
[11] A. Y. Fadeev, T. J. McCarthy, *Langmuir* **1999**, *15*, 7238–7243.
[12] T. L. Sun, L. Feng, X. F. Gao, L. Jiang, *Acc. Chem. Res.* **2005**, *38*, 644–652.
[13] L. Zhai, M. C. Berg, F. C. Cebeci, Y. Kim, J. M. Milwid, M. F. Rubner, R. E. Cohen, *Nano Lett.* **2006**, *6*, 1213–1217.
[14] T. Nishino, M. Meguro, K. Nakamae, M. Matsushita, Y. Ueda, *Langmuir* **1999**, *15*, 4321–4323.
[15] L. Ionov, *J. Mater. Chem.* **2010**, *20*, 3382–3390.
[16] M. A. C. Stuart, W. T. S. Huck, J. Genzer, M. Muller, C. Ober, M. Stamm, G. B. Sukhorukov, I. Szleifer, V. V. Tsukruk, M. Urban, F. Winnik, S. Zauscher, I. Luzinov, S. Minko, *Nat. Mater.* **2010**, *9*, 101–113.
[17] J. A. Howarter, J. P. Youngblood, *Adv. Mater.* **2007**, *19*, 3838–3843.
[18] J. Lahann, S. Mitragotri, T. N. Tran, H. Kaido, J. Sundaram, I. S. Choi, S. Hoffer, G. A. Somorjai, R. Langer, *Science* **2003**, *299*, 371–374. .
[19] K. Ichimura, S. K. Oh, M. Nakagawa, *Science* **2000**, *288*, 1624–1626.
[20] N. L. Abbott, C. B. Gorman, G. M. Whitesides, *Langmuir* **1995**, *11*, 16–18.
[21] B. S. Gallardo, V. K. Gupta, F. D. Eagerton, L. I. Jong, V. S. Craig, R. R. Shah, N. L. Abbott, *Science* **1999**, *283*, 57–60.
[22] G. M. Whitesides, B. Grzybowski, *Science* **2002**, *295*, 2418–2421.
[23] S. Park, J. H. Lim, S. W. Chung, C. A. Mirkin, *Science* **2004**, *303*, 348–351.
[24] Z. Y. Tang, N. A. Kotov, S. Magonov, B. Ozturk, *Nat. Mater.* **2003**, *2*, 413–418.
[25] B. J. Hinds, N. Chopra, T. Rantell, R. Andrews, V. Gavalas, L. G. Bachas, *Science* **2004**, *303*, 62–65.
[26] M. Zhang, S. L. Fang, A. A. Zakhidov, S. B. Lee, A. E. Aliev, C. D. Williams, K. R. Atkinson, R. H. Baughman, *Science* **2005**, *309*, 1215–1219.
[27] H. B. Xia, D. Y. Wang, *Adv. Mater.* **2008**, *20*, 4253–4256.
[28] J. Jin, Y. Wakayama, X. S. Peng, I. Ichinose, *Nat. Mater.* **2007**, *6*, 686–691.
[29] T. E. Gier, X. Bu, P. Feng, G. D. Stucky, *Nature* **1998**, *395*, 154–157.
[30] G. Gu, M. Schmid, P. W. Chiu, A. Minett, J. Fraysse, G. T. Kim, S. Roth, M. Kozlov, E. Munoz, R. H. Baughman, *Nat. Mater.* **2003**, *2*, 316–319.
[31] J. Yuan, K. Laubernds, J. Villegas, S. Gomez, S. L. Suib, *Adv. Mater.* **2004**, *16*, 1729–1732.
[32] X. S. Peng, J. Jin, Y. Nakamura, T. Ohno, I. Ichinose, *Nat. Nanotechnol.* **2009**, *4*, 353–357.
[33] J. K. Yuan, X. G. Liu, O. Akbulut, J. Q. Hu, S. L. Suib, J. Kong, F. Stellacci, *Nat. Nanotechnol.* **2008**, *3*, 332–336.
[34] Y. F. Qiu, D. F. Liu, J. H. Yang, S. H. Yang, *Adv. Mater.* **2006**, *18*, 2604–2608.
[35] J. Shieh, F. J. Hou, Y. C. Chen, H. M. Chen, S. P. Yang, C. C. Cheng, H. L. Chen, *Adv. Mater.* **2010**, *22*, 597–601.
[36] Q. Fu, G. V. R. Rao, S. B. Basame, D. J. Keller, K. Artyushkova, J. E. Fulghum, G. P. López, *J. Am. Chem. Soc.* **2004**, *126*, 8904–8905.
[37] X. J. Feng, L. Jiang, *Adv. Mater.* **2006**, *18*, 3063–3078.
[38] X. Z. Ren, *College Physics* **2005**, *24*, 10–11.
[39] M. J. Bojan, W. A. Steele, *Carbon* **1998**, *36*, 1417–1423.
[40] A. Han, G. Mondin, N. G. Hegelbach, N. F. de Rooij, U. Staufer, *J. Colloid Interface Sci.* **2006**, *293*, 151–157.

Received: August 4, 2010
Published online: November 24, 2010

